

# Shear Band Patterns in Metallic Glasses under Static Indentation, Dynamic Indentation, and Scratch Processes

GHATU SUBHASH and HONGWEN ZHANG

The deformation structure in terms of shear band patterns in bulk metallic glasses (BMGs) under static indentation, dynamic indentation, and dynamic scratch tests has been investigated. The evolved shear band patterns appear to be a strong function of loading rate, although the plastic regions beneath the loading surface have similarities in shape irrespective of loading type. Comparison of currently available modeling estimates with experimental measurements has revealed that these models predict the plastic zone size reasonably well at low loads but deviate considerably at higher loads. The variation in spacing of shear bands is rationalized on the basis of the shear displacement accommodated by the shear bands formed under different loading rates, which results from a proposed shear-band formation mechanism based on the momentum diffusion model.

DOI: 10.1007/s11661-007-9315-2

© The Minerals, Metals & Materials Society and ASM International 2007

## I. INTRODUCTION

UNLIKE many traditional engineering materials, bulk metallic glasses (BMGs) have been developed as a scientific curiosity rather than for a specific need.<sup>[1]</sup> Therefore, this class of materials is yet to find widespread engineering applications. The excellent mechanical properties of BMGs such as high strength (1.4 GPa for Pt-based BMGs to above 4 GPa for FeCo-based BMGs),<sup>[2]</sup> high elastic limits ~2 pct, and wide range of fracture toughness 10 to 100 MPa · m<sup>1/2</sup><sup>[1]</sup> have been widely recognized. The deformation behavior of BMGs under nanoindentation,<sup>[3]</sup> microindentation,<sup>[4]</sup> flexural loads,<sup>[5]</sup> and uniaxial compression<sup>[6]</sup> and tension<sup>[7]</sup> has also been well studied in the literature. Although the inelastic deformation is known to occur in the form of shear bands, the nature of these shear band patterns is yet to be fully explored under a wide variety of loading scenarios.

Improvements in the processing technology of BMGs have rapidly progressed in the last few decades from being able to make thin ribbons to large rods of diameter beyond 10 mm.<sup>[8,9]</sup> Innovative manufacturing methods and technologies are being adopted to make usable components from these BMGs for aerospace engineering and defense applications. Machining using a single-point tool is often one of the popular manufacturing methods to shape BMGs into complex parts.

---

GHATU SUBHASH, Professor, is with the Department of Mechanical and Aerospace Engineering, University of Florida, Gainesville, FL 32611-6250. Contact e-mail: subhash@ufl.edu  
HONGWEN ZHANG, Postdoctoral Candidate, is with the Department of Materials Science and Engineering, Michigan Technological University, Houghton, MI 49931.

This article is based on a presentation made in the symposium entitled "Dynamic Behavior of Materials," which occurred during the TMS Annual Meeting and Exhibition, February 25–March 1, 2007 in Orlando, Florida, under the auspices of The Minerals, Metals and Materials Society, TMS Structural Materials Division, and TMS/ASM Mechanical Behavior of Materials Committee.

Article published online September 13, 2007

However, research into this particular aspect of BMGs is scarce, probably due to the limitations in the geometrical size of the specimens that can be obtained. Fundamental insights into the behavior of BMGs under machining conditions can be obtained by modeling their response under single-point loads. Such studies are well documented on metals<sup>[10]</sup> and brittle materials,<sup>[11]</sup> where, as a first step, the interaction between a single-point tool and a workpiece is modeled as an indentation event with the indenter penetrating the specimen in the normal direction while being dragged in the lateral direction. Typical static indentation experiments impose only normal loads. Extension of these experiments to single-point scratch loads allows for superposition of both normal and tangential loads. This loading scenario is expected to mimic the interaction of a single-point tool with the work piece during a machining operation and can provide insight into the fundamental material removal process.

Numerous studies have focused on the indentation response of BMGs. The serrated flow observed in load-displacement curves during nanoindentation<sup>[3]</sup> has been attributed to the development of individual shear bands beneath the indentation. However, observations on the loading (top) surface of the specimen revealed only a few shear bands, which cannot account for the large ductility observed in the quasi-static indentation.<sup>[4]</sup> Therefore, Ramamurthy *et al.*<sup>[12]</sup> and Zhang *et al.*<sup>[4]</sup> have used the bonded interface technique to observe the shear band patterns beneath a static microindentation. They noted numerous shear bands to evolve within the inelastic zone. The size of this zone also increased with indentation load.

Although static indentation studies are of fundamental value to understand the evolving shear band patterns beneath an indentation, they do not capture the rate-dependent deformation response that is germane to high rate loading events such as impact or high speed machining. Under dynamic loading, BMGs are known to exhibit the same or lower uniaxial fracture strength

compared to their static counterpart values.<sup>[13–16]</sup> This behavior is contrary to the known response in metals and ceramics, where an increase in the uniaxial fracture strength with strain rate has been traditionally noted.<sup>[17,18]</sup> Recently, Subhash and Zhang<sup>[16]</sup> conducted dynamic indentation experiments and presented data on the reduction in hardness in BMGs at higher strain rates and compared these results to the reduction in dynamic uniaxial fracture strength as a function of strain rate. In the current article, we will present evolved shear band patterns under static and dynamic indentations and then extend such investigations to scratch studies. Similarities and differences between the evolved shear band patterns will be discussed.

## II. EXPERIMENTAL METHOD

Cylindrical ingots of  $Zr_{57}Cu_{15.4}Ni_{12.6}Al_{10}Nb_5$  alloy of 3 mm diameter were used in current investigations. Indentation and scratch experiments were performed on bonded cylindrical specimens.<sup>[4]</sup> In this technique, the cylindrical specimens were first cut vertically into two halves and the cut surfaces were then polished to mirror finish. They were then bonded using epoxy resin and held tightly in a fixture. The resulting interface thickness was around  $6\ \mu\text{m}$ .<sup>[4]</sup> The top loading surface of this composite specimen was also polished flat for indentation studies. Vickers indentations were then conducted with the indenter diagonal aligned parallel to the interface. Static and dynamic indentations were performed at equivalent loads for comparison of evolved shear band patterns. Static experiments were conducted at different loads with a loading duration of 15 seconds. The dynamic indentations were conducted using a dynamic indentation hardness tester described in earlier publications by Subhash and co-workers.<sup>[16,19–21]</sup> The duration of dynamic loading was around  $100\ \mu\text{s}$ . The strain rate of indentation was estimated to be above  $1000/\text{s}$ .<sup>[16]</sup> After the experiments, the bonded specimens were separated to observe the evolved patterns beneath the indentations.

The scratch experiments were conducted using a custom-designed scratch tester, shown in Figure 1, used for fundamental studies of material removal in metals and ceramics by Subhash and co-workers.<sup>[11,22,23]</sup> A single-point conical (90 deg included angle) diamond dressing tool is used as the scratch tool. The tool is held in a pendulum that is supported by two precision ball bearings housed in a steel fixture. The bonded split specimen rests on a high-frequency load transducer that is screwed into a special holder in the steel fixture so that the normal force during the scratch process can be measured *in situ* and recorded on a digital oscilloscope. The tip of the diamond tool is held in contact with the specimen before the scratch event. The top of the pendulum is pushed by a pneumatic piston to create a scratch in the form of a circular arc on the specimen surface. The maximum depth of cut (DOC) during the scratch as well as the location of the scratch on the specimen surface can be adjusted with reasonable precision with several micrometers positioned in the

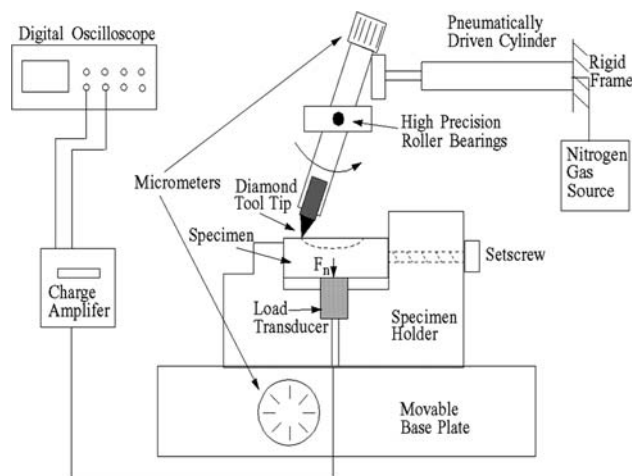


Fig. 1—Schematic of the experimental setup for scratch testing.

steel fixture.<sup>[11]</sup> Scratches were conducted along and across the bonded interface. The evolved shear band patterns on the top surface (along the banks of the scratch groove) and beneath the scratch were observed using a scanning electron microscope.

## III. RESULTS

Typical deformation structures after a static indentation, a dynamic indentation, and a dynamic scratch test on the loading surfaces (top surface) of different specimens are shown in Figure 2. It is seen from the indentation imprint in Figure 2(a) that the inside region of a static indentation is devoid of deformation features (as evident from the smooth indented region). On the other hand, the dynamically indented regions reveal cracks along the circular slip steps of shear bands and even peel-off cracks, as shown in Figure 2(b).<sup>[4,16]</sup> Figure 2(c) reveals the profile of a single scratch groove. The interior of the groove is quite smooth, which implies ductile mode of deformation during the scratch process.<sup>[10,23]</sup> At higher magnification, numerous slip steps of shear bands have been observed along the banks on either side of the groove, as shown in Figure 3. At the entry and exit of the scratch (where the DOC is shallower than that in the middle of the scratch groove), only one set of shear bands, inclined at around 10 and 30 deg to the scratch direction and with a spacing of 300 to 500 nm, have been observed (Figure 3(a)). In the middle of a scratch groove where the DOC is high, Figure 3(b) illustrates two sets of shear bands, intersecting each other, on the banks of the scratch groove. One set of shear bands have similar spacing (300 to 500 nm) and inclination angle to those observed around the end of the scratch groove (as in Figure 3(a)), while the second set of shear bands have much wider spacing (2 to 4  $\mu\text{m}$ ) and are inclined to the scratch direction at a 60 to 80 deg angle. In addition, numerous machining-chip like features have also been observed in the groove, as shown in Figure 3(c), which further confirm that the deformation behavior of this particular BMG under

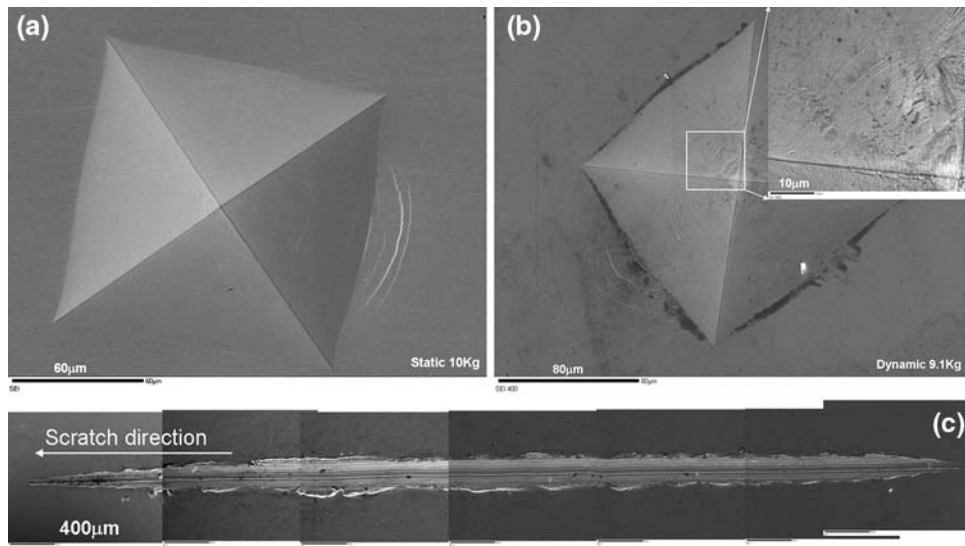


Fig. 2—Deformation structure on the top surface of (a) a static indentation, (b) a dynamic indentation, and (c) a dynamic scratch.

single-point scratching is more like the traditional metals<sup>[10]</sup> rather than the brittle materials.<sup>[11]</sup>

Deformation structures beneath the loading surfaces, obtained from separating the bonded specimens, are shown in Figure 4. Beneath the static indentation (Figure 4(a)), multiple sets of slip steps of shear bands have been observed. Numerous semicircular shear bands with an average spacing of 200 to 300 nm are seen. In addition, a second set of a small number of disconnected shear bands, symmetrically arranged on both sides of indentation, with varying spacing but at significantly greater spacing than the primary semicircular shear bands are seen. On the other hand, dynamic indentations produce two types of semicircular shear bands surrounding the indentation with different spacing and different curvatures, as shown in Figure 4(b). The maximum spacing for the inner shear bands ranges from 3 to 10  $\mu\text{m}$ , while the spacing for the outer ones varies from 0.4 to 3  $\mu\text{m}$ . It is also noted that the shear band spacing right beneath the indentation is larger but gradually decreases toward the top surface. Finally, the slip steps of the shear bands beneath a scratch that is formed parallel to the interface of the split specimen are illustrated in Figure 4(c). Notice that shear bands evolve parallel to each other, and the depth of this plastic zone size remains almost constant (around 17  $\mu\text{m}$ ) for the entire length of the scratch. The average spacing of these shear bands is around  $\sim 3.5 \mu\text{m}$ .

Figure 5 displays the shear band pattern at the tip of a scratch on one of the split specimens when the scratch was conducted across a junction (bonded interface) of two split specimens. After the test, the two split specimens have been separated to view the shear band patterns on one of the half specimens. The inverted V-shaped groove is the scratch, and the shear bands can be seen to emanate from the tip of the scratch and propagate toward the top surface. This shear band pattern is different from those observed beneath the static and dynamic indentations shown

earlier, which may indicate that evolved shear band patterns not only depend on the geometry of the tool but also on the imposed stress state. In indentation experiments, only normal load is imposed whereas in the scratch process, both normal and tangential loads are imposed. The moving scratch tool initiates the shear bands at the tip, and then these bands propagate to the top surface. The spacing of these shear bands right beneath the groove is also around 3.5  $\mu\text{m}$ , which is similar to the spacing of shear bands observed in Figure 4(c). Recall the secondary shear bands identified on the banks of the scratch groove on the top surface in Figure 3(b). The similarity of these shear band spacings together with the observation that they extend to the top surface may possibly indicate that these shear bands belong to the same system and have similar origin.

## IV. DISCUSSION

### A. Plastic Zone Size

The micrographs presented in Figures 3 through 5 clearly reveal that the plastic zone in BMGs due to indentation and scratch processes is characterized by various sets of shear bands beneath the surface. The size of this plastic zone or the extent of shear band containing region depends mainly on the nature of load, loading rate, geometry of the tool tip, *etc.* An estimate of the size of this inelastic region is of interest for modeling the deformation behavior BMGs accurately. Expanding cavity models<sup>[24]</sup> have been widely used for the estimation of plastic zone size in a wide variety of materials including ceramics<sup>[25]</sup> and BMGs.<sup>[4]</sup> In this model, the radius of the plastic zone  $b$  (from the center of the indentation on the top surface to the boundary of the region containing shear bands) has been found to depend primarily on contact area radius  $a$

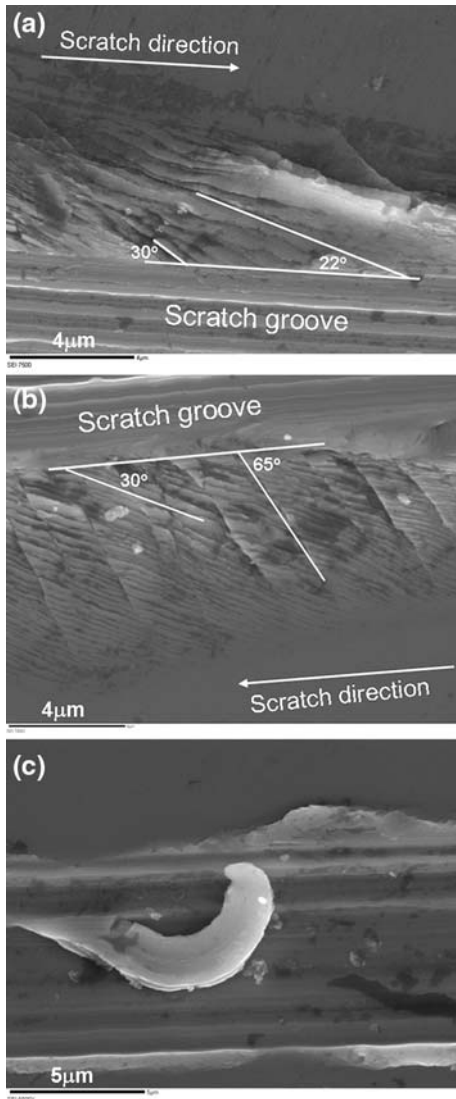


Fig. 3—Shear band pattern on the banks of a scratch groove for (a) shallower DOC and (b) deeper DOC. (c) Machining-chip like feature on the scratch groove.

(radius of the imprint on the top surface), indenter geometry (*i.e.*, half apex angle  $\beta$  of the indenter), and material properties such as Young's modulus  $E$ , density  $\rho$ , and Poisson's ratio  $\nu$ , as

$$\frac{b}{a} = \left[ \frac{E}{6(1-\nu) \cdot \sigma_y} \cot \beta + \frac{2}{3} \left( \frac{1-2\nu}{1-\nu} \right) \right]^{1/3} \quad [1]$$

Giannakopoulos and Suresh<sup>[26]</sup> also developed a finite-element-based model for estimation of plastic zone size due to indentation by

$$\frac{b}{a} = \sqrt{\frac{0.3\pi H}{\sigma_y^c}} \quad [2]$$

where  $H$  is the hardness and  $\sigma_y^c$  is the compressive yield strength. Based on single-crystal plasticity, Zieliński<sup>[27]</sup> estimated the plastic zone size as

$$\frac{b}{a} = \sqrt{\frac{3H}{2\sigma_y^c}} \quad [3]$$

Our intent is to compare the preceding model estimates of plastic zone size with the experimental measurements from a large number of tests on this BMG. Comparison between the model predictions and the experimental data is shown in Figure 6. It is observed that the predictions of plastic zone size from all three models agree well with the experimental data from low-depth (small contact size) processes but deviate considerably from the observed values at higher-depth processes. Three main reasons are identified for this deviation. (1) Use of average hardness value in modeling work. As reported in Reference 4, the hardness of this particular BMG decreases with increasing load and tends to approach a stable value at higher loads. (2) The rate-dependent hardness has not been considered in the preceding models. It is now well recognized that BMGs exhibit negative rate sensitivity of hardness and fracture strength (*i.e.*, softening behavior) at high strain rates.<sup>[15,16,28]</sup> Both the dynamic indentation and scratch process are high rate deformation processes, and the use of appropriate rate-dependent properties are necessary to capture the experimentally observed trends in plastic zone size in BMGs. (3) The preceding models are phenomenological and do not account for the fundamental deformation mechanisms of BMGs, *i.e.*, pressure-sensitive yield, viscous flow associated with the shear band formation, *etc.* Therefore, more sophisticated models are needed to fully capture such complex features observed under various loading scenarios in BMGs.

## B. Mechanism of Shear Band Formation

In the following, we will propose a mechanism for shear band formation in BMGs. In dynamic indentation and scratch experiments, shear bands can form in sub-microsecond durations, and therefore, the local strain rate within the shear bands can be very high. Typical models based on quasi-static deformation mechanisms cannot fully capture the shear band evolution process. To describe such dynamic growth phenomena, a momentum diffusion model is more appropriate. This particular model has widely been used by many researchers to study shear behavior in solids undergoing high-strain-rate deformation.<sup>[29,30]</sup> In BMGs, the decrease of viscosity by several orders of magnitude during shear band evolution has been predicted.<sup>[31]</sup> In addition, BMGs are pressure sensitive,<sup>[15,16]</sup> and the effects of normal pressure on their deformation behavior must be accounted for. Considering these issues, we intend to illustrate a basic mechanism that may be applicable for shear band formation in BMGs.

Figure 7 illustrates a schematic of the shear band evolution mechanism. Under the applied loading, a small material volume experiences shear stress  $\tau$  as well as normal stress  $\sigma_N$  (to account for pressure-sensitive behavior<sup>[15,16,31]</sup>), as shown in Figure 7(a). Due to large defect distribution in BMGs (recall that BMGs have

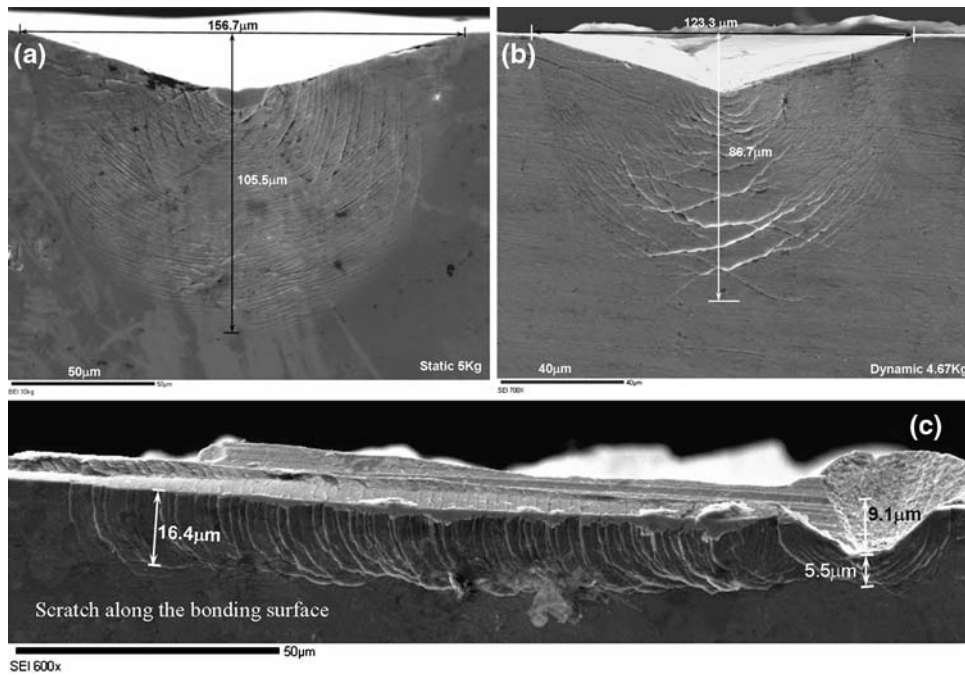


Fig. 4—Shear band pattern on split specimens beneath (a) a static indentation, (b) a dynamic indentation, and (c) a dynamic scratch.

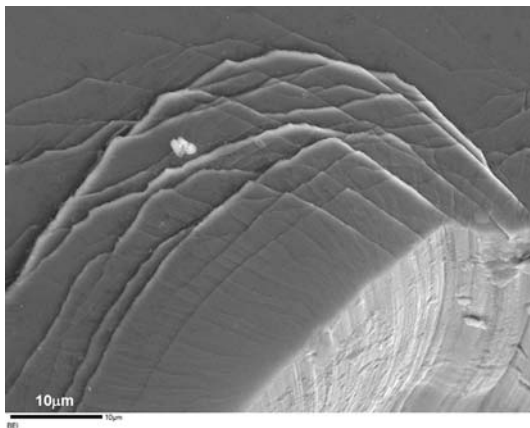


Fig. 5—Shear bands emanating from the tip of a scratch tool.

disordered structure), shear band initiates immediately at some favorable location, causing the adjacent regions to slide. This process unloads the shear stress in the core of the shear band to the adjacent regions (Figure 7(b)). Thus, the momentum associated with the high rate of loading and the associated deformation is diffused to the neighboring region. The width  $\zeta$  of this unloaded region (*i.e.*, shear relaxed region) grows along with shear displacement  $\psi$  across the shear band, until the momentum in the shear relaxed region becomes constant (*i.e.*, velocity  $V$  becomes constant in the entire region) and the shear stress  $\tau$  at the core of the shear band is reduced to zero. Upon reaching a critical shear displacement, the shear band is fully formed, as depicted in Figure 7(c). The larger the shear displacement across the shear band, the greater will be the width over which the momentum diffuses and hence the wider will be the spacing between

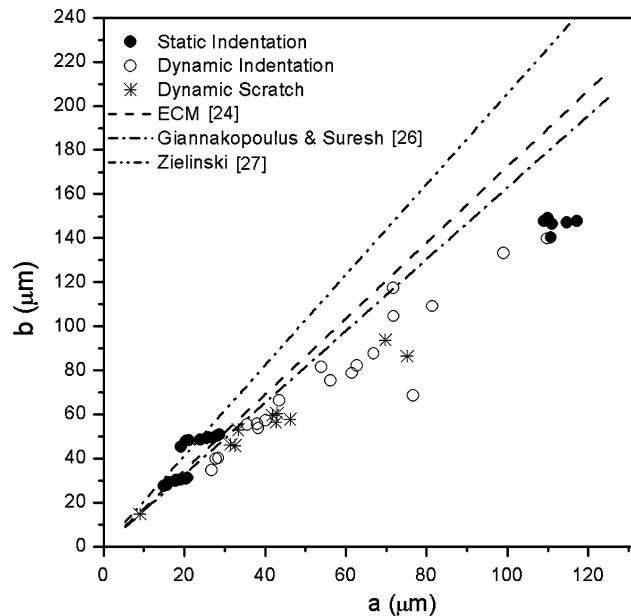


Fig. 6—Comparison of experimentally measured plastic zone sizes with available models.

two adjacent shear bands. With continued loading, the undeformed adjacent region will start to undergo a similar shear banding process.

Clearly, the model suggests that shear band spacing is dependent on the shear displacement accommodated during shear band evolution. The larger the shear displacement, the wider will be the spacing, and *vice versa*. Conner *et al.*<sup>[5]</sup> have also reported a similar dependence of shear band spacing on the plastic strain under bending, where the shear band spacing continues

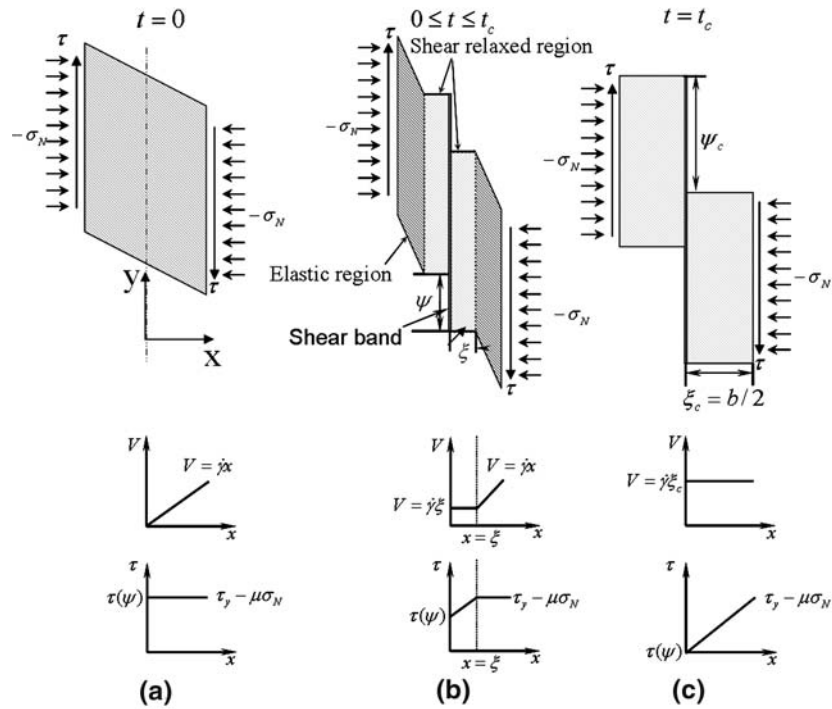


Fig. 7—Schematic of the momentum diffusion model for shear band evolution.

to increase until the inelastic strain is fully accommodated. This idea can be used to rationalize the current observation of larger shear band spacing under dynamic indentation and scratch processes compared to static indentations (Figure 4). Under dynamic indentation, the number of shear bands is less than that in static indentation, and more severe deformation features are observed inside the dynamic indent (Figure 2(b)). From these observations, it is concluded that higher plastic strain would be accommodated by the shear bands formed under dynamic deformation than under static deformation. Therefore, a wider spacing would be expected under dynamic deformation. Thus, the preceding preliminary model helps to explain the deformation patterns in a simplistic way. More in-depth mechanistic analysis based on the preceding mechanism will be presented in future publications.

## V. CONCLUSIONS

Observations of shear band patterns under static indentation, dynamic indentation, and dynamic scratch processes in a BMG revealed that the spacing of shear bands under dynamic processes is greater than in a static process. The deformation is also more severe under dynamic indentation compared to static indentation. These features have been rationalized based on a momentum diffusion mechanism where the shear band spacing is argued to be proportional to the magnitude of shear displacement across a shear band. The current models available in the literature do not adequately capture the plastic zone size in BMGs. Loss of strength and hardness at high strain rates and load dependence of

hardness have been argued to be the probable causes for deviation in model prediction compared to experimental results. It is suggested that more in-depth modeling efforts and rate-dependent material properties are required to capture the realistic behavior of BMGs under various loading scenarios.

## ACKNOWLEDGMENTS

This work was partially supported by the Weapons and Materials Research Directorate, United States Army Research Laboratory (Aberdeen Proving Ground, MD). Partial support was also provided for the development of a dynamic indenter by the NSF (Grant No. CMS-0324461), Dr. Ken Chong, Program Manager. The BMG specimens were supplied by Dr. Laszlo Kecskes, United States Army Research Laboratory (Aberdeen Proving Ground).

## REFERENCES

1. M.F. Ashby and A.L. Greer: *Scripta Mater.*, 2006, vol. 54, pp. 321–26.
2. H.W. Zhang, G. Subhash, X.N. Jing, L.J. Kecskes, and R.J. Dowding: *Philos. Mag. Lett.*, 2006, vol. 86, pp. 333–45.
3. C.A. Schuh and T.G. Nieh: *J. Mater. Res.*, 2004, vol. 19, pp. 46–57.
4. H.W. Zhang, X.N. Jing, G. Subhash, L.J. Kecskes, and R.J. Dowding: *Acta Mater.*, 2005, vol. 53, pp. 3849–59.
5. R.D. Conner, W.L. Johnson, N.E. Paton, and W.D. Nix: *J. Appl. Phys.*, 2003, vol. 94, pp. 904–11.
6. T.C. Hufnagel, T. Jiao, Y. Li, L.-Q. Xing, and K.T. Ramesh: *J. Mater. Res.*, 2002, vol. 17, pp. 1441–45.

7. B. Yang, M.L. Morrison, P.K. Liaw, R.A. Buchanan, G. Wang, C.T. Liu, and M. Denda: *Appl. Phys. Lett.*, 2005, vol. 86, p. 141904.
8. A. Peker and W. Johnson: *Appl. Phys. Lett.*, 1993, vol. 63, pp. 2342–44.
9. A. Inoue, N. Nishiyama, and T. Matsuda: *Mater. Trans. JIM*, 1996, vol. 37, pp. 181–84.
10. H. Wang, G. Subhash, and A. Chandra: *Wear*, 2001, vol. 249, pp. 566–81.
11. G. Subhash, M.A. Marszalek, and S. Maiti: *J. Am. Ceram. Soc.*, 2006, vol. 89, pp. 2528–36.
12. U. Ramamurty, S. Jana, Y. Kawamura, and K. Chattopadhyay: *Acta Mater.*, 2005, vol. 53, pp. 705–17.
13. H.A. Bruck, A.J. Rosakis, and W.L. Johnson: *J. Mater. Res.*, 1996, vol. 11, pp. 503–11.
14. G. Subhash, R. Dowding, and L. Kecskes: *Mater. Sci. Eng.*, 2002, vol. A334, pp. 33–40.
15. H. Li, G. Subhash, X.L. Gao, L.J. Kecskes, and R.J. Dowding: *Scripta Mater.*, 2003, vol. 49, pp. 1087–92.
16. G. Subhash and H.W. Zhang: *J. Mater. Res.*, 2007, vol. 22, pp. 478–85.
17. M.A. Meyers, V.F. Nesterenko, J.C. LaSalvia, and Q. Xue: *Mater. Sci. Eng.*, 2001, vol. A317, pp. 204–25.
18. G. Subhash and G. Ravichandran: *ASM Handbook*, vol. 8, *Mechanical Testing and Evaluation*, ASM INTERNATIONAL, Materials Park, OH, 2000, pp. 497–504.
19. B.J. Koeppel and G. Subhash: *Wear*, 1999, vol. 224, pp. 56–67.
20. G. Subhash: *ASM Handbook*, vol. 8, *Mechanical Testing and Evaluation*, ASM INTERNATIONAL, Materials Park, OH, 2000, pp. 519–29.
21. D. Ghosh, G. Subhash, T. Sudarshan, G. Radhakrishnan, and X.-L. Gao: *J. Am. Ceram. Soc.*, 2007, vol. 90, pp. 1850–57.
22. G. Subhash and R. Bandyo: *J. Am. Ceram. Soc.*, 2005, vol. 88, pp. 918–25.
23. G. Subhash, J.E. Loukus, and S.M. Pandit: *Mech. Mater.*, 2002, vol. 34, pp. 25–42.
24. K.L. Johnson: *J. Mech. Phys. Solids*, 1970, vol. 18, pp. 115–26.
25. X.-L. Gao, X.N. Jing, and G. Subhash: *Int. J. Solids Struct.*, 2006, vol. 43, pp. 2193–2208.
26. A.E. Giannakopoulos and S. Suresh: *Scripta Mater.*, 1999, vol. 40, pp. 1191–98.
27. W. Zielinski, H. Huang, and W.W. Gerberich: *J. Mater. Res.*, 1993, vol. 8, pp. 1300–10.
28. C.A. Schuh, T.C. Hofnagel, and U. Ramamurty: *Acta Mater.*, 2007, vol. 55, pp. 4067–4109.
29. D.E. Grady and M.E. Kipp: *J. Mech. Phys. Solids*, 1987, vol. 35, pp. 95–118.
30. M.E. Kipp and D.E. Grady: *J. Mech. Phys. Solids*, 1985, vol. 33, pp. 399–415.
31. H.W. Zhang, G. Subhash, and S. Maiti: *J. Appl. Phys.*, 2007, vol. 102, p. 043519.